Optical waveguides formed by silver ion exchange in Schott SG11 glass for waveguide evanescent field fluorescence microscopy: evanescent images of HEK293 cells

Abdollah Hassanzadeh
University of Western Ontario
Department of Physics and Astronomy
London, Ontario, Canada N6A 3K7
  and
University of Kurdistan
Department of Physics
Sanandaj, Iran

Michael Nitsche
University of Western Ontario
Department of Physics and Astronomy
London, Ontario, Canada N6A 3K7
  and
University of Applied Sciences Wiesbaden
Department of Physics
Am Brückweg 26
65428 Rüsselsheim, Germany

Souzan Armstrong
University of Western Ontario
Schulich School of Medicine & Dentistry
Department of Physiology and Pharmacology
London, Ontario, Canada N6A 5C1

Noushin Nabavi
Rene Harrison
University of Toronto Scarborough
Department of Cell and Systems Biology
1265 Military Trail
Toronto, Ontario, Canada M1C 1A4

S. Jeffrey Dixon
University of Western Ontario
Schulich School of Medicine & Dentistry
Department of Physiology and Pharmacology
London, Ontario, Canada N6A 5C1

Uwe Langbein
University of Applied Sciences Wiesbaden
Department of Physics
Am Brückweg 26
65428 Rüsselsheim, Germany

Address all correspondence to Silvia Mittler, Department of Physics and Astronomy, University of Western Ontario, London, Ontario, Canada N6A 3KL. Tel: (519) 661-2111 loc. 88592; Fax: (519) 661-2033; E-mail: smittler@uwo.ca.

Silvia Mittler
University of Western Ontario
Department of Physics and Astronomy
London, Ontario, Canada N6A 3K7

Abstract. Planar glass waveguides with a specific number of modes were fabricated by Ag^+-Na^+ exchange in Schott SG11 glass. The effective refractive indices were determined using m-line spectroscopy in both s- and p-polarization. By using the reversed Wentzel–Kramers–Brillouin approximation, the index profiles were described by a nonlinear diffusion equation. The diffusion coefficients for Ag^+ were established, as well as the penetration depth of the evanescent field in an aqueous environment for the different modes. The integrals of $|E|^2$ fields for the evanescent-guided fields were investigated. These are important when evanescent fields are used for illumination in interface microscopy, an alternative method to total internal reflection fluorescence (TIRF) microscopy. The photoluminescent behavior of the waveguides was investigated as a function of ion exchange time and excitation wavelengths. Comparable images were obtained of fluorescently labeled HEK293 cells using TIRF microscopy and waveguide evanescent field fluorescence microscopy. Imaging was performed using HEK293 cells, delivering similar images and information. © *2010 Society of Photo-Optical Instrumentation Engineers.* [DOI: 10.1117/1.3443796]

1 Introduction

Exchanging ions with a low polarizability and small size (e.g., Na^+) with ions of high polarizability and large size (Ag^+) in a glass slide leads to a region of high refractive index that can serve as an optical waveguide.[1] In 1972, Izawa and Nakagome[2] first reported on ion-exchanged waveguides by Tl^+ in silicate glass containing oxides of sodium and potassium. Since then, ion-exchanged waveguides have been fabricated using various ions, such as Ag^+, K^+, Li^+, Rb^+, Cs^+, Cu^+, and Tl^+; salts, such as $AgNO_3$, $TlNO_3$, $CsCl$, $NaNO_3$, and KNO_3; salt mixtures such as $CsNO_3-CsCl$, KNO_3-AgNO_3, $AgNO_3-NaNO_3$, and $CuSO_4-Na_2SO_4$, (Ref. 3); and several different glasses, such as soda-lime, BGG21, borosilicate, Schott BK7, aluminisilicate, and Corning 0211 (Refs. 1, 4, and 5).

Waveguides fabricated by ion exchange have taken on an important role in many applications, such as sensors,[6,7] nonlinear integrated optical switches,[8] and evanescent scattering microscopy.[9] In the present study, we introduce a glass that shows a very high diffusion constant for Ag ions and apply the fabricated waveguides to waveguide evanescent field fluorescence (WEFF) microscopy.[9–14] This is an inexpensive alternative to total internal reflection fluorescence (TIRF) microscopy.[15] Images of cell–substratum contact regions of HEK293 cells were obtained using WEFF microscopy and compared to images obtained using classical TIRF microscopy.

We have established an ion-exchange protocol to fabricate waveguides with a defined number of modes. With the help of m-line spectroscopy,[16,17] we characterized the fabricated waveguides with respect to the effective refractive indices, the effects of exchange-time and temperature, and the diffusion profiles and the temperature-dependent diffusion coefficient of the silver ions. The penetration depths of the evanescent field for different modes were calculated. The integral of the intensity of the evanescent field was investigated for transverse electric (TE) and transverse magnetic (TM) modes. Ag$^+$ ions, Ag aggregates, and nanoparticles can be present in such ion-exchanged waveguides and can lead to photoluminescence.[18–24] Therefore, fluorescence emission spectra excited at different laser lines were recorded. Usually in fluorescence microscopy, background signals such as autofluorescence of the substrate are avoided, but in the case of waveguide microscopy, they can be used as an internal standard for normalizing the coupling efficiency during analysis of intensity data.[24]

2 Experimental

2.1 Ion Exchange

Glass slides of SG11 (SCHOTT, Grünenplan, Germany) with a thickness of 1.85 mm cut into 15 mm $\times$ 25 mm pieces were first sonicated in 2% Hellmanex (Hellma, Berlin, Germany) solution for 15 min and then rinsed 20 times with Milli-Q water (Milli-Q, $\rho > 18$ MΩcm, Millipore) and sonicated in Milli-Q water for 20 min. Next, the slides were rinsed 20 times with ethanol (anhydrous, Sigma Aldrich), sonicated in ethanol for 15 min, and dried with nitrogen gas. The cleaned glass slides were placed on top of molten salt in a custom-made glass spoon at a fixed temperature in a tube furnace (Yokogawa M&C Corporation, Tokyo, Japan). This allowed ion exchange to happen only at the interface of the glass and molten salt. The ion-exchange temperature and the diffusion time were varied from 225 °C to 400 °C and from 4 min to hours, respectively.

After the ion exchange, the glass was removed from the melt, cooled with nitrogen gas under ambient conditions, thoroughly rinsed with Milli-Q water, and sonicated for 30 min in Milli-Q water. Cooling the glass slides with nitrogen gas helped to control the ion-exchange time, especially when the time is small.

2.2 m-Line Spectroscopy with Prism Coupling

Waveguide coupling was performed using a home-built prism coupling setup in m-line geometry. The prism, a 90-deg

LASFN9 (Berliner Glass GmbH, Germany, with refractive index $n = 1.84489$ at $\lambda = 632.8$ nm) pressed on the waveguide, was turned by a computer-controlled motorized stage (Newport). The coupling angles were determined by detecting the light intensity at the end face of the waveguide using a biased photodiode (Siemens BPW 34 B) during a θ-angle scan. When the laser beam on the prism's surface reflects back onto itself, the laser beam is perpendicular to the prism's surface and θ equals zero. This was used as the reference angle. A scheme of the experimental setup can be found in Refs. [16] and [25]. The accuracy in measuring the synchronous angles using this method is about $\pm 1'$. This inaccuracy in the synchronous angle yields an inaccuracy of $\pm 1 \times 10^{-4}$ in the measurement of the effective refractive index, N_{eff}. A linearly polarized HeNe laser (JDS Uniphase, $\lambda = 632.8$ nm, 20 mW) was used for exciting the waveguide modes.

2.3 Fluorescence Emission Spectra and Loss Measurements

As previously found in studies of ion-exchanged waveguides,[18–24] silver ions, molecules, clusters, and nanoparticles can cause optical electronic waveguide losses due to fluorescence excitation. When the evanescent field of the coupled light for a particular guided wavelength is designed to illuminate samples located on the waveguide (e.g., to carry out evanescent field fluorescence microscopy), additional fluorescence photons of a different wavelength are undesirable. However, they can be used as an internal intensity standard. Typically, coupling efficiencies to waveguides are not known without thorough investigation; therefore, an intrinsic light signal from the fluorescence of the waveguide can be useful for intensity calibrations.[26]

For optical loss measurements, polarized light of an argon ion laser (Melles Griot), with various laser lines from 454 to 519 nm and maximum output powers from 12 to 130 mW in both TE and TM polarizations, were coupled individually into the waveguides by a photoresist coupling grating.[27] The intensity profile of the fluorescence light streak was viewed with an inverted microscope (Zeiss, Axiovert 25) and a digital camera (Diagnostic Instruments, Inc., Sterling Heights, Michigan) with frame-grabber software (Image Pro Express from Media Cybernetics, Bethesda, Maryland). Appropriate filters (dielectric long pass, Omega Optics) were used to filter the excitation wavelength propagating in the waveguide. The losses were calculated in dB/cm by analyzing the exponential decay of the emitted fluorescence light along the waveguide streak measured by means of the frame grabber software.

For obtaining the emission spectra of the excited Ag ions and agglomerates in the waveguide, fluorescence photons were collected along the streak by the microscope and spectrally analyzed by an adapted spectrometer via an optical fiber (Ocean Optics, Dunedin, Florida, HR-2000 spectrometer).

2.4 Determination of Penetration Depth of the Evanescent Field

The penetration depth of the evanescent intensity was quantified as the depth where the evanescent field dropped to 1/e of the intensity directly at the waveguide surface. The penetration depths of the different modes in the waveguide in both

TE and TM polarizations were estimated from simulations of the field distribution, especially the evanescent field on top of the waveguide in an aqueous environment ($n = 1.33$). The measured refractive index profile was implemented into the simulations. These simulations were performed by a commercially available software package called TRAMAX,[28] which uses a transfer matrix formalism based on the Fresnel equations. The wavelength was chosen to be $\lambda = 632.8$ nm. To compare the evanescent fields directly and to be independent of experimental coupling conditions, all modes (TE modes) were normalized to their entire field integral along the three-layer waveguide structure.

2.5 Cell Preparation

HEK293 cells are a transformed human embryonic kidney cell line.[29] Culture medium consisted of Dulbecco's modified eagle medium (DMEM high glucose) supplemented with 10% heat-inactivated fetal bovine serum (FBS) and antibiotics (penicillin 100 units/ml, streptomycin 100 μg/ml, amphotericin B 0.25 μg/ml; Invitrogen, Burlington, Ontario). Waveguides were presoaked for at least 5 min in culture medium. Medium was then removed, and the cells were seeded directly on the waveguide. After 24 h incubation in 5% CO_2/95% air at 37 °C, samples were washed with phosphate-buffered saline (PBS) to remove any nonviable cells and loaded with fluorescent lipophilic probe 1,1′-dioctadecyl-3,3,3′,3′-tetramethylindocarbocyanine perchlorate (DiI, Invitrogen) according to manufacturer's instructions. The cells were imaged in phenol red-free DMEM (Invitrogen).

2.6 TIRF Microscopy

For TIRF microscopy, DiI-stained HEK293 cells were placed in Attofluor cell chambers (Molecular Probes, Eugene, Oregon) and positioned on the heated stage of a Zeiss inverted microscope (Axiovert 200M) equipped with a Zeiss TIRF slider. The filter set used (Zeiss 53) consisted of an excitation filter (509 to 519 nm), a dichroic mirror FT 540, and an emission bandpass filter (550 to 600 nm). Images were captured with a Zeiss Plan-Fluar $100 \times / 1.45$ oil-immersion objective lens at excitation wavelength of 514 nm from a multiline argon ion laser (100 mW). The images were recorded by a cooled CCD camera (AxioCam MR, Zeiss). With this microscope, epifluorescence and TIRF microscopy images can be taken of the same specimen by changing the angle of incidence on the coverslip. The optimal angle used for TIRF was approximately 61 deg.

2.7 Waveguide Evanescent Field Fluorescence Microscopy

For imaging cell–substrate contact regions by waveguide evanescent field fluorescence microscopy, the stage of an inverted microscope (Zeiss, Axiovert 25) was modified to accommodate an xy-stage and a sample stage.[11,13,14] A beam from a HeNe laser at a wavelength of 543 nm and an output power of 0.5 mW was coupled via a photoresist grating (grating constant $\Lambda = 665$ nm) into the ion-exchanged waveguide that was located on the sample stage of the microscope. The images were taken with a $40 \times$ objective. A 560-nm long-pass filter (3DR470LP, Omega Optics) was used for collecting the
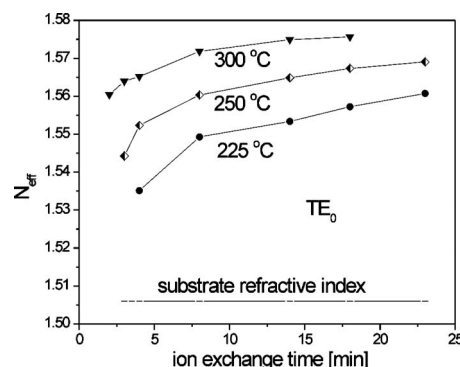

Fig. 1 Effective refractive indices (N_{eff}) at $\lambda = 632.8$ nm of TE_0 modes for three different exchange temperatures versus the ion exchange time. The horizontal line represents the substrate refractive index of Schott SG11.

fluorescence emission from the DiI dye. A digital camera (Diagnostic Instruments, Inc., Sterling Heights, Michigan) with imaging software (Image Pro Express, Media Cybernetics, Bethesda, Maryland) was used for capturing the images on a computer.

3 Results and Discussion

All fabricated waveguides were characterized with m-line spectroscopy. Using the measured coupling angles (θ_m), the effective refractive indices (N_{eff}), of both TE and TM modes were calculated.[30] With increasing ion-exchange time at fixed temperature, the number of guided modes and the N_{eff} of a given mode increase, as previously reported.[24] Figure 1 depicts the effect of ion-exchange time and temperature on N_{eff} for the TE_0 modes of various multimode waveguides. It is evident that by increasing time or temperature, N_{eff} of a specific mode will increase. The results for higher order modes are similar (not shown).

We used the reversed Wentzel–Kramers–Brillouin (WKB)[31] method for constructing the refractive index profile in the ion-exchanged glass waveguides from a set of identified N_{eff}. These profiles were then fitted successfully with a nonlinear diffusion profile proposed in Ref. 32, as demonstrated in Ref. 24;

$$n(x) = n_s + \frac{\Delta n}{\gamma}[1 - (1 - \gamma)^{erfc(x/d_{eff})}], \quad (1)$$

$$\gamma = \alpha N, \quad \alpha = 1 - \frac{D_{Ag}}{D_{Na}}. \quad (2)$$

Here, n_s is the refractive index of the substrate, Δn is the maximum increase in the refractive index at the surface, N is the portion of exchanged ions, D_{Ag} and D_{Na} are the diffusion coefficients of Ag^+ and Na^+, respectively, and d_{eff} is the effective diffusion depth. The effective diffusion depth, d_{eff}, is given by the relationship
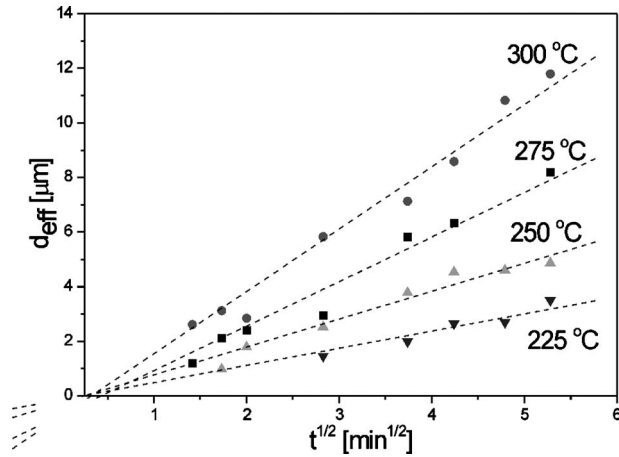
Fig. 2 Effective diffusion depth (d_{eff}) versus the square root of the ion exchange time (t) for TE modes.

$$d_{eff} = 2\sqrt{D_e t}, \qquad (3)$$

where t is the diffusion time or ion-exchange time, and D_e is the effective diffusion constant. The temperature dependence of D_e below the glass transition temperature can be fitted to an Arrhenius equation:[5,33,34]

$$D_e = C_1 e^{(-C_2/T)}. \qquad (4)$$

Hence, from Eqs. (2)–(4), we find

$$d_{eff} = C_1' t^{1/2} e^{(-C_2'/T)}, \qquad (5)$$

with t the time in minutes, and T the temperature in Kelvin. C_1' and C_2' are constants.

Figure 2 depicts the linear behavior of the simulated d_{eff} versus $\sqrt{t}$ for TE modes of various samples fabricated with pure silver nitrate. Table 1 summarizes the effective diffusion constant data (D_e), obtained from Eqs. (2) and (3). With increasing temperature, the effective diffusion constant D_e is increasing as depicted in Fig. 3 in the ($\ln D_e$) versus ($1/T$) plot. With a linear fit, we determine $C_1^{\text{TE}} = 1.77 \times 10^{-6}$ m^2 s^{-1} and $C_2^{\text{TE}} = 1.01 \times 10^4$ K. By introducing the universal gas constant R, the effective diffusion constant can be written in terms of an activation energy ΔE:

Table 1 Measured surface refractive index change Δn and effective diffusion constant D_e as a function of exchange temperature T.

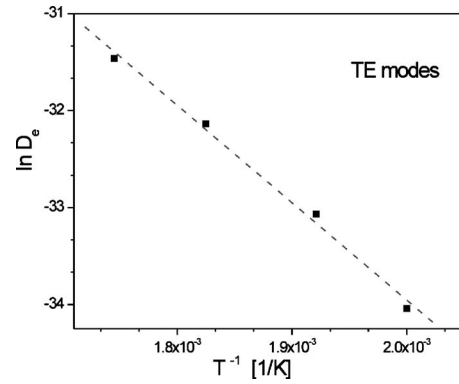| T [°C]	$\Delta n (\times 10^{-3})$	D_e [m^2/s] $\times 10^{-16}$
225	82 ± 2	16.49
250	84 ± 4	43.56
275	84 ± 2	110.50
300	85 ± 4	216.76

Fig. 3 Dependence of the effective diffusion coefficient (D_e) on temperature (T).

$$D_e = 7.98 \cdot 10^3 e^{-\Delta E/RT}. \qquad (6)$$

By comparing Eqs. (4) and (6) and using $C_2^{\text{TE}} = 1.01 \times 10^4$ K, the activation energy can be found as $\Delta E = 8.40 \times 10^4$ J mole^{-1}. The effective diffusion depth with a given temperature and time and the effective diffusion constant for a given temperature can be obtained by using Eqs. (5) and (6) and constants C_1 and C_2.

Table 1 also shows the surface refractive index change (Δn) at the four different exchange temperatures. It can be seen that by increasing the temperature, Δn increases, whereas it is known that Δn is independent from the diffusion time.[1,3] By comparing the results for the diffusion coefficients of Ag ions in SG11 with those for Ag ions in BK7,[35] Ag ions were found to have a much larger diffusion coefficient in SG11.

To use the waveguides for evanescent illumination purposes, precise knowledge about the evanescent field is needed—especially the penetration depth and the carried intensity in the illuminating field. The penetration depth of modes of a particular waveguide (for fabrication parameters of the waveguide, see legend) into the cover medium (here, water with a refractive index of $n = 1.33$) increases with increasing mode number with a slight off-bend toward higher mode numbers and ranged between 40 to 45 nm (Fig. 4). The
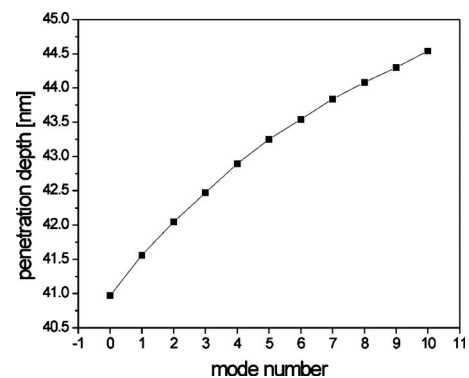

Fig. 4 Penetration depth of the evanescent field versus mode number for TE modes. The ion exchange time and temperature were 18 min and 300 °C, respectively. The salt was pure AgNO$_3$.
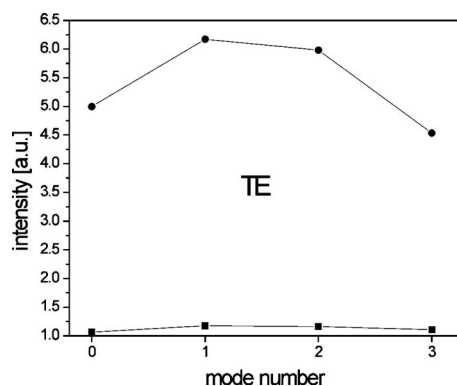
Fig. 5 Normalized integrated intensity in the cover medium [$I = \int |E|^2$(evanescent field)$dx / \int |E|^2$(total field)dx] versus mode number for two salt concentrations (-●- 100% AgNO$_3$ and -■- 1% AgNO$_3$ +99% KNO$_3$). Ion exchange parameters: 100% AgNO$_3$ ($T=260$ °C, $t=11$ min); AgNO$_3$+KNO$_3$ mixture ($T=370$ °C, $t=35$ min).

influence of the silver concentration in the waveguide fabrication process on the intensity of the guided light in the evanescent field is shown in Fig. 5. The normalized integrated intensity I, calculated via the integrals of $|E|^2$ fields for the evanescent-guided fields, is plotted for two different four-mode waveguides as a function of the mode number. One waveguide was fabricated with pure AgNO$_3$, and the other by a mixture of 1% AgNO$_3$ and 99% KNO$_3$. The pure AgNO$_3$ waveguide showed much higher integrated intensity in the evanescent field.

It is known that Ag ion exchange can lead to yellow-stained glasses due to absorption and photoluminescence (PL).[18–24] Therefore, the fluorescence behavior of waveguides fabricated with pure silver salt and two different exchange times t_e was investigated. Figure 6 shows fluorescence emission spectra taken at four excitation wavelengths (488 nm, 477 nm, 470 nm, and 454 nm). The fluorescence emission spectra for the 510-s sample show contributions of two to three peaks, with a systematic highest peak at low wavelength (or high energy) and smaller peaks on the lower energy side [Fig. 6(a)]. The 1200-s sample shows less structured peaks but a systematic red shift in emission peak position with decreasing photon excitation energy [Fig. 6(b)]. The coupling conditions into the waveguide mode were not controlled; therefore, the peak amplitudes cannot be compared. The effect of ion-exchange time on the formation of Ag compounds, aggregates, and possibly nanoparticles of various sizes and size distributions are the reason for this spectral behavior.[18–23]

The losses of these waveguides were also investigated. Losses were found to depend on the fabrication procedure, the mode number, the polarization, and the wavelength propagating in the guide. Losses on the order of 1.2 to 7.8 dB/cm were observed, with loss values being typically larger for the higher number modes and smaller for lower number modes.

3.1 TIRF and Waveguide Evanescent Field Fluorescence Microscopy

To compare the waveguide evanescent field fluorescence microscopy with well-established TIRF microscopy, HEK293 cells were seeded on ion-exchanged waveguides and on TIRF coverslips and stained with DiI. Figure 7 shows a round and
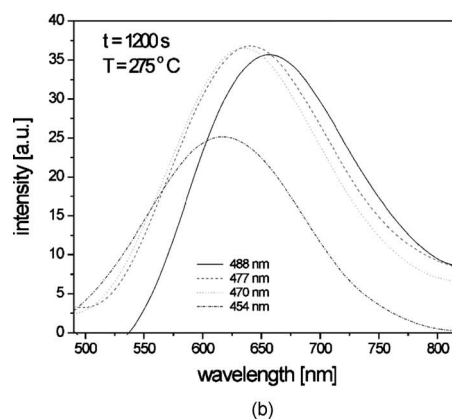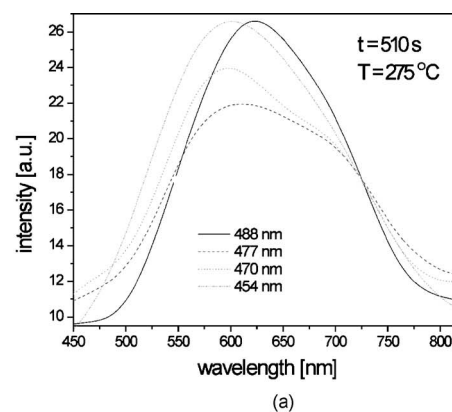

(a)

(b)

Fig. 6 Fluorescence emission spectra taken at four excitation wavelengths (labeled in graph) for a randomly chosen mode of a waveguide fabricated with pure silver salt at 275 °C with (a) $t_e=510$ s and (b) $t_e=1200$ s of ion exchange.

an elongated HEK293 cell. The left panels (a) and (b) are epifluorescence images, whereas the right panels (c) and (d) depict corresponding TIRF microscopy images. In the epifluorescence mode, the entire cell is depicted, showing high-intensity areas where dye accumulation occurs. In the TIRF
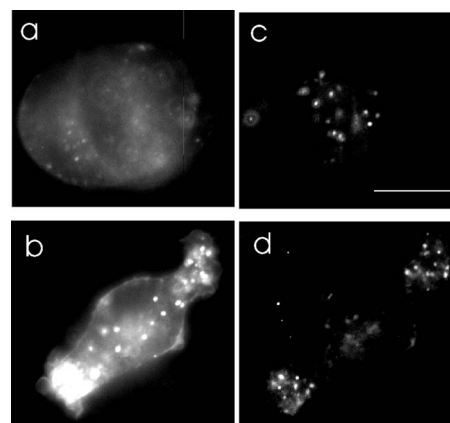

Fig. 7 Classical epifluorescence and TIRF microscopy with a Zeiss TIRF microscope on HEK293 cells stained with DiI. Two cells are shown. The left panels, (a) and (b), show epifluorescence, and the right panels, (c) and (d), the corresponding TIRF images of the two cells. The scale bar is 10 μm.
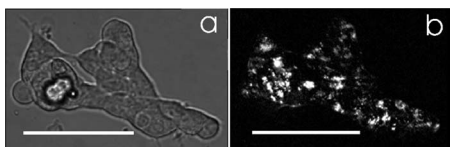
Fig. 8 (a) Bright-field image and (b) waveguide evanescent field fluorescence image of DiI-stained HEK293 cells. The scale bar is 40 μm. Due to the lower magnification objective used in the waveguide experiments, the pixels of the camera chip give an impression of square-shaped focal adhesions. This is an artifact.

mode, only focal regions of close contact between the cell membrane and the coverslip are visible. The different intensities here are due to a convolution of dye concentration and distance from the coverslip surface.

The waveguide evanescent field fluorescence image of similarly prepared HEK293 cells is depicted together with a bright-field image of these cells in Fig. 8 at a smaller magnification. In WEFF microscopy, a $40\times$ objective was used due to the lack of a $100\times$ objective. However, comparing images without investigating resolution issues is straightforward. The waveguide evanescent image reveals regional contacts of various cells with similar high contrast as in the TIRF images.

Images published so far obtained with waveguide evanescent field fluorescence microscopy often show—besides the evanescent image—contributions from epifluorescence. These contributions are produced by light scattered from the waveguides. This scattered light is able to excite fluorescent dyes outside the evanescent field in all parts of the cell that are stained. This leads to a weak but visible fluorescence emission of the entire cell's plasma membrane. Therefore, the outlines of the cells can often be seen as weak, but additional, information in these mixed images. In Fig. 8 (WEFF), these areas of enhanced emission due to scattering are seen as the gray structures visible throughout the cell. This is in contrast to the crisp, mainly dot-like evanescent structures in the TIRF images [Fig. 7(c) and 7(d)]. However, some scattering signal is evident in the TIRF images of Fig. 7 as well, leading to the grayish areas at locations where high dye concentration or cellular structures are detected in the epiflorescence mode.

The fine-tuning of the WEFF technology to achieve pure evanescent images or to achieve a controlled mixture of evanescent and scattering controlled epifluorescent images is still under development.[36] In TIRF microscopy, two images can be taken at two different TIRF angles to yield a set of information—the entire cell and the focal regions of close contact. However, this takes time. In WEFF microscopy, on the other hand, images can be taken quickly with both sets of information in one image. This will be of advantage, when dynamic studies are performed and fast kinetic data are required.

Despite the losses and the autofluorescence of the waveguide, high-quality evanescent images could be obtained with the ion-exchanged SG11 waveguides showing the same quality with respect to contrast as in the TIRF images.

4 Conclusion

Schott SG11 glass was used to fabricate waveguides as substrates for waveguide evanescent field fluorescence micros-

copy. It depicts all the necessary features of ion exchange but offers a much higher diffusion coefficient for Ag ions in comparison to standard glasses such as BK7 or soda-lime glasses. One can therefore fabricate waveguides as a microscopy substrate very economically at low temperatures and short exchange times. However, due to the high diffusion constant, these waveguide substrates cannot be autoclaved for disinfection. The heat will change the diffusion profile of the ions and therefore the optical performance. Therefore, chemical disinfection is required prior to seeding cells. Despite the autofluorescence that these waveguides show due to silver cluster formation and the losses associated with this effect, waveguide evanescent field fluorescence microscopy of HEK293 cells was successful. It compares very well with evanescent images taken from the same cells with a conventional TIRF microscope.

References

1. R. V. Ramaswamy and R. Srivastava, "Ion-exchanged glass waveguides—a review," *J. Lightwave Technol.* **6**(6), 984–1002 (1988).
2. T. Izawa and H. Nakagome, "Optical waveguide formed by electrically induced migration of ions in glass plates," *Appl. Phys. Lett.* **21**(12), 584–586 (1972).
3. T. Findakly, "Glass waveguide by ion-exchange: a review," *Opt. Eng.* **24**(2), 244–250 (1985).
4. S. I. Najafi, *Introduction to Glass Integrated Optics*, Artech House, Boston, London (1992).
5. F. Gonella, "Characterization of Cu–Na ion-exchanged glass waveguides," *Appl. Phys. Lett.* **69**(3), 314–315 (1996).
6. D. S. Walker, W. M. Reichert, and C. J. Berry, "Corning 7059, silicon oxynitride, and silicon dioxide thin-film integrated optical waveguides—in search of low-loss, nonfluorescent reusable glass waveguides," *Appl. Spectrosc.* **46**(9), 1437–1441 (1992).
7. W. Lukosz, "Integrated optical chemical and direct biochemical sensors," *Sens. Actuators B* **29**(1–3), 37–50 (1995).
8. S. Honkonen, S. I. Najafi, W.-J. Wang, P. Lefebvre, M.-J. Li, and A. Tervonen, "Single-mode glass channel waveguides by ion-exchange with ionic masking," *Opt. Commun.* **94**(1–3), 54–58 (1992).
9. H. M. Grandin, B. Städtler, M. Textor, and J. Vörös, "Waveguide excitation fluorescence microscopy: a new tool for sensing and imaging the biointerface," *Biosens. Bioelectron.* **21**(8), 1476–1482 (2006).
10. R. Horvath, H. C. Pedersen, N. D. Selmeczi, and N. B. Larsen Skivesen, "Monitoring of living cell attachment and spreading using reverse symmetry waveguide sensing," *Appl. Phys. Lett.* **86**, 071101 (2005).
11. A. Hassanzadeh, M. Nitsche, S. Armstrong, J. Dixon, U. Langbein, and S. Mittler, "Waveguide evanescent field fluorescence microscopy: thin film fluorescence intensities and its application in cell biology," *Appl. Phys. Lett.* **92**(23), 233503 (2008).
12. B. Agnarsson, S. Ingthorsson, T. Gudjonsson, and K. Leosson, "Evanescent-wave fluorescence microscopy using symmetric planar waveguides," *Opt. Express* **17**(7), 5075–5082 (2009).

13. A. Hassanzadeh, S. Armstrong, S. J. Dixon, and S. Mittler, "Multi-mode waveguide evanescent field fluorescence microscopy: measurement of cell-substratum separation distance," *Appl. Phys. Lett.* **94**(3), 033503 (2009).

14. A. Hassanzadeh, H. Kan Ma, S. Armstrong, S. J. Dixon, S. M. Sims, and S. Mittler, "Waveguide evanescent field fluorescence microscopy: from cell-substratum distances to kinetic cell behavior," *Proc. SPIE* **7322**, 73220A (2009).

15. D. Axelrod, E. H. Hellen, and R. M. Fulbright, "Total internal reflection fluorescence," in *Topics in Fluorescence Spectroscopy*, Vol. **3**, Biochemical Application, J. R. Lakowicz, Ed., pp. 289–343, Plenum Press, New York (1992).

16. F. Thoma, U. Langbein, and S. Mittler-Neher, "Waveguide scattering microscopy," *Opt. Commun.* **134**(1–6), 16–20 (1997); F. Thoma, J. Armitage, H. Trembley, B. Menges, U. Langbein, and S. Mittler-Neher, "Waveguide scattering microscopy in air and water," *Proc. SPIE* **3414**, 242–249 (1998).

17. M. J. Adams, *An Introduction to Optical Waveguides*, John Wiley, New York (1981); R. G. Hunsperger, *Integrated Optics: Theory and Technology*, 4th ed., Springer, Berlin, New York (1995); T. Tamir ed., "Integrated optics," in *Topics in Applied Physics*, vol. **7**, 2nd ed., Springer, Heidelberg, New York (1979). A. W. Snyder and J. D. Love, Optical Waveguide Theory, Chapman and Hall, London, New York (1983); D. Marcuse, *Theory of Dielectric Optical Waveguides*, 2nd ed., Academic Press, Boston (1991).

18. G. T. Boyd, Z. H. Yu, and Y. R. Shen, "Photoinduced luminescence from the noble-metals and its enhancement on rough surfaces," *Phys. Rev. B* **33**(12), 7923–7936 (1986).

19. J. Zheng and R. M. Dickson, "Individual water-soluble dendrimer-encapsulated silver nanodot fluorescence," *J. Electron. Mater.* **124**(47), 13982–13983 (2002).

20. A. Abdullah and S. Annapoorni, "Fluorescent silver nanoparticles via exploding wire technique," *Pramana, J. Phys.* **65**(5), 815–819 (2005).

21. J. A. Jimenez, S. Lysenko, G. Zhang, and H. Liu, "Optical characterization of Ag nanoparticles embedded in aluminophosphate glass," *J. Electron. Mater.* **36**(7), 812–820 (2007).

22. J. Hu, W. Lee, W. Cai, L. Tong, and H. Zeng, "Evolution of the optical spectra of an Ag mesoporous SiO_2 nanostructure heat-treated in air and H_2 atmospheres," *Nanotechnology* **18**(18), 185710 (2007).

23. P. Gangopadhyay, R. Kesavamoorthy, S. Bera, P. Magudapathy, K. G. M. Nair, B. K. Panigrahi, and S. V. Narasimhan, "Optical absorption and photoluminescence spectroscopy of the growth of silver nanoparticles," *Phys. Rev. Lett.* **94**(4), 047403 (2005).

24. M. Weisser, F. Thoma, B. Menges, U. Langbein, and S. Mittler-Neher, "Fluorescence in ion exchanged BK7 glass slab waveguides and its use for scattering free loss measurements," *Opt. Commun.* **153**(1–3), 27–31 (1998).

25. T.-M. Lee, S. Mittler-Neher, D. Neher, G. I. Stegeman, C. Roux, M. Leclerc, J. Martin, and S. I. Najafi, "Side-chain dilution effect on the optical properties of poly[3-alkylthiophene]s," *Opt. Mater.* **1**, 65–70 (1992).

26. S. Monneret, P. Huguet-Chantome, and F. Flory, "*m*-lines technique: prism coupling measurement and discussion of accuracy for homogeneous waveguides," *J. Opt. A, Pure Appl. Opt.* **2**(3), 188–195 (2000).

27. X. Mei, R. Moshrefzadeh, U. J. Gibson, G. I. Stegeman, and C. T. Seaton, "Simple versatile method for fabricating guided-wave gratings," *Appl. Opt.* **24**, 3155–3161 (1985).

28. TRAMAX, University of Jena, Institute of Theoretical Optics, Max Wien Platz 1, 07743 Jena, Germany.

29. F. L. Graham, J. Smiley, W. C. Russell, R. Nairn, "Characteristics of a human cell line transformed by DNA from human adenovirus type 5," *J. Gen. Virol.* **36**, 59–74 (1977).

30. R. Ulrich and R. Torge, "Measurement of thin-film papameters with prism coupler," *Appl. Opt.* **12**(12), 2901–2908 (1973).

31. J. M. White and P. F. Heidrich, "Optical-waveguide refractive-index profiles determined from mode indexes—simple analysis," *Appl. Opt.* **15**(1), 151–155 (1976).

32. J. Linares, X. Prieto, and C. Montero, "A novel refractive-index profile for optical characterization of nonlinear diffusion-processes and planar waveguides in glass," *Opt. Mater.* **3**(4), 229–236 (1994).

33. G. Stewart, C. A. Miller, P. J. R. Laybourn, C. D. W. Wilkinson, and R. M. De LaRue, "Planar optical waveguides formed by silver-ion migration in glass," *IEEE J. Quantum Electron.* **13**(4), 192–200 (1977).

34. R. H. Doremus, "Ion exchange in glass," in *Ion Exchange—A Series of Advances*, vol. **2**, J. A. Marinsky, Ed., pp. 1–42, Marcel Dekker, New York (1969).

35. R. G. Eguchi, E. A. Maunders, and I. K. Naik, "Fabrication of low-loss waveguides in BK7 by ion-exchange," *Proc. SPIE* **408**, 21–26 (1983).

36. D. Imruck, "Evanescent field waveguide fluorescence microscopy of cells on biopolymers," Diploma Thesis, University of Applied Sciences, Wiesbaden, Germany (2009).